IEEE Photonics Journal
An IEEE Photonics Society Publication

Open Access

Impact of Stimulated Raman Scattering on the Transverse Mode Instability Threshold

Volume 10, Number 3, June 2018

Zebiao Li
Chengyu Li
Yu Liu
Qiang Luo
Honghuan Lin
Zhihua Huang
Shanhui Xu
Zhongmin Yang
Jianjun Wang
Feng Jing

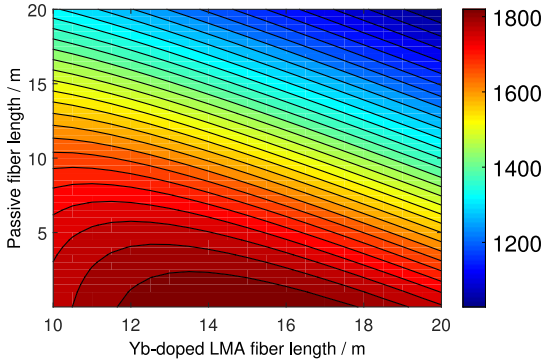

DOI: 10.1109/JPHOT.2018.2842467
1943-0655 © 2018 IEEE

IEEE photonics SOCIETY

IEEE

Impact of Stimulated Raman Scattering on the Transverse Mode Instability Threshold

Zebiao Li,[1,2] **Chengyu Li**,[2] **Yu Liu**,[2] **Qiang Luo**,[2] **Honghuan Lin**,[2] **Zhihua Huang**,[2] **Shanhui Xu**,[1] **Zhongmin Yang**,[1] **Jianjun Wang**,[2] **and Feng Jing**[2]

[1]South China University of Technology, State Key Laboratory of Luminescent Materials and Devices and Institute of Optical Communication Materials, Guangzhou 510640, China
[2]China Academy of Engineering Physics, Research Center of Laser Fusion, Mianyang 621900, China

DOI:10.1109/JPHOT.2018.2842467

Manuscript received April 18, 2018; revised May 22, 2018; accepted May 28, 2018. Date of publication June 4, 2018; date of current version June 13, 2018. This work was supported in part by the National Science Foundation of China under Grants 11474257, 11404305, 11674103, 61635004, and 61535014; in part by the National Key Research and Development Program of China under Grant 2017YFB1104401; in part by the Fundamental Research Funds for Central Universities under Grants 2015ZM091 and 2017BQ002; in part by the China National Funds for Distinguished Young Scientists under Grant 61325024; in part by the Guangdong Natural Science Foundation under Grants 2016A030310410 and 2017A030310007; and in part by the Science and Technology Project of Guangdong under Grants 2014B050505007, 2015B090926010, 2016B090925004, and 2017B090911005. Corresponding author: Zebiao Li (e-mail:zebiaolee@163.com).

Abstract: Quantum defect originating from the stimulated Raman scattering (SRS) effect is a heat source that induces refractive index grating and, thus, significantly decreases the threshold of transverse mode instability (TMI), which is the main limiting factor for the power scaling of high-power fiber lasers. A semi-analytical model that takes the TMI and SRS effects into account was developed, and the impact of the Raman content variation due to changes in the injected seed and fiber length on the TMI threshold was investigated. Experimental demonstrations of the impact of the SRS effect on the TMI threshold are presented. We proved that TMI affects the beam quality of the signal light rather than the Raman light. Taking these facts into account, the suppression of SRS could be an effective way to counter the TMI of fiber lasers.

Index Terms: Transverse mode instability, stimulated Raman effect, fiber laser.

1. Introduction

Most recently, transverse mode instability (TMI) has attracted attention because it is responsible for the beam quality degradation of fiber lasers reaching a power threshold, and is therefore a limiting factor for the power scaling of high-power fiber lasers with a nearly diffraction-limited beam [1], [2]. Quantum defect between the pump and the signal light is the main reason of TMI; the thermally-induced refractive index grating couples the power from the fundamental mode to the first higher-order mode [3], [4]. Besides, it was found in experiments that the photo-darkening (PD) effect could also induce TMI [5], [6]. A number of modeling works have been done accordingly, demonstrating that PD losses are a second heat source greatly influencing TMI threshold [7], [8]. A detailed analysis on the behavior of the quasi-static TMI effect is presented in [9].

Highly-doped customized fibers usually suffer from high PD losses and, thus, a low TMI threshold. Commercial standard large-mode-area (LMA) fibers, on the other hand, exhibit lower PD losses, but also a still evident TMI effect [10]. Indeed, commercial fibers have comparatively lower pump absorption due to their smaller mode field, so longer pieces of gain fiber are needed to ensure pump depletion, which might intensify the stimulated Raman scattering (SRS) effect. It has been demonstrated that Raman conversion could cause TMI in Raman fiber lasers [11]. In previous research [12], we found that as the length of the beam delivery fiber after the fiber amplifier increased, the TMI effect was enhanced along with the Raman content in the laser output. Therefore, it is reasonable to suppose the TMI effect is related to the SRS effect in LMA fiber lasers.

In this paper, both theoretical and experimental works are presented to demonstrate that the quantum defect originating from SRS is a heat source that induces TMI effect as well. For the first time, to the best of our knowledge, a semi-analytical model that takes the TMI and SRS effects together into account was developed, and it was proven that the Raman content and the TMI threshold are negatively correlated: an increase of the former is followed by a significant decrease of the latter. Besides, we experimentally found that, it is the signal light rather than the Raman light, the one that suffers from beam quality degradation. A number of strategies are proposed and discussed for suppressing the SRS effect so as to increase the TMI threshold of fiber lasers.

2. Simulation Model and Results

A semi-analytical model was built to study the behavior of the SRS effect in high-power fiber lasers. For commercial standard Yb-doped LMA fibers, the PD losses and the background losses are normally quite low. Hence, in order to simplify the physical process and to reduce the computational complexity, only the heat generated from quantum defect (due to pump-signal conversion) and the SRS effect (due to signal-Raman conversion) were taken into account in the laser model. Apart from these, gain saturation, which could reduce the TMI threshold [13], was also included. The heat source in the proposed model can be written as follows:

$$Q \cong \left(\frac{v_p}{v_s}-1\right)\frac{g_0}{1+I_p/\Gamma_p I_p^{sat}+I_s/I_s^{sat}}\left(I_s+\frac{\bar{I}\left(1+I_p/\Gamma_p I_p^{sat}\right)}{1+I_p/\Gamma_p I_p^{sat}+I_s/I_s^{sat}}\right)+g_R\left(\frac{v_s}{v_R}-1\right)I_R I_s \tag{1}$$

In this equation, subscript p, s and R denote the pump light, signal light, and Raman light, respectively, while superscript *sat* represents the saturation power. I is optical intensity and v is optical frequency. Γ is the overlapping factor. g_0 is the small signal gain and g_R is the Raman gain coefficient. With this heat source equation, the temperature distribution along the fiber can be obtained. To simulate the power evolution along the gain fiber, the propagation equations of the pump light, signal light, and Raman light are given, respectively, in (2b)–(2d), while the upper level population derived from steady-state rate equations is expressed in (2a) [14]–[16].

$$\frac{N_2(z)}{N_{Yb}}=\frac{\frac{\Gamma_p\sigma_{ap}P_p}{hv_pA_{clad}}+\frac{\Gamma_s\sigma_{as}P_s}{hv_sA_{core}}+\frac{\Gamma_R\sigma_{aR}P_R}{hv_RA_{eff}}}{\frac{\Gamma_p(\sigma_{ap}+\sigma_{ep})P_p}{hv_pA_{clad}}+\frac{\Gamma_s(\sigma_{as}+\sigma_{as})P_s}{hv_sA_{core}}+\frac{\Gamma_R(\sigma_{aR}+\sigma_{eR})P_R}{hv_RA_{eff}}} \tag{2a}$$

$$\frac{dP_p(z)}{dz}=-\Gamma_p\left[\sigma_{ap}N_{Yb}-\left(\sigma_{ap}+\sigma_{ep}\right)N_2(z)\right]P_p(z)+2\Gamma_p\sigma_{ep}N_2(z)\frac{hc^2}{\lambda_p^3}\Delta\lambda \tag{2b}$$

$$\frac{dP_s(z)}{dz}=-\Gamma_s\left[\sigma_{as}N_{Yb}-\left(\sigma_{as}+\sigma_{es}\right)N_2(z)\right]P_s(z)+2\Gamma_s\sigma_{es}N_2(z)\frac{hc^2}{\lambda_s^3}\Delta\lambda-\frac{\lambda_R}{\lambda_s}\frac{g_R}{A_{eff}}P_R(z)P_s(z) \tag{2c}$$

$$\frac{dP_R(z)}{dz} = -\Gamma_R\left[\sigma_{aR}N_{Yb} - (\sigma_{aR}+\sigma_{eR})N_2(z)\right]P_R(z) + 2\Gamma_R\sigma_{eR}N_2(z)\frac{hc^2}{\lambda_R^3}\Delta\lambda + \frac{g_R}{A_{eff}}P_R(z)P_s(z) \tag{2d}$$

In these equations, subscript a and e denote the absorption cross section and the emission cross section, respectively. A represents area and λ is optical wavelength. N_2 is the upper state population while N_{Yb} is doped ions concentration. Using the Helmholtz equation with a slowly varying amplitude approximation and considering gain saturation, the coupled mode equations can be obtained as [12], [17]–[19]

$$\frac{\partial P_1}{\partial z} = -\tilde{\chi}_1(\Omega)\tilde{g}P_1P_2 - \chi_2(\Omega)g_R\frac{P_R}{A_{eff}}P_1P_2 + \Gamma_1\tilde{g}P_1 \tag{3a}$$

$$\frac{\partial P_2}{\partial z} = \tilde{\chi}_1(\Omega)\tilde{g}P_1P_2 + \chi_2(\Omega)g_R\frac{P_R}{A_{eff}}P_1P_2 + \Gamma_2\tilde{g}P_2 \tag{3b}$$

$$\tilde{\chi}_1(\Omega) = \chi_1(\Omega)\frac{1+P_p/P_p^{sat}}{1+P_p/P_p^{sat}+P_s/P_s^{sat}} \tag{3c}$$

$$\chi_1(\Omega) = \frac{2k_0\alpha\eta}{\kappa}\left(\frac{\nu_p}{\nu_s}-1\right)\mathrm{Im}\left(\sum_{\upsilon}\sum_{m=1}^{\infty}\frac{4n_0^2\varepsilon_0^2c^2}{\pi(\alpha\beta_m^2-j\Omega)}\frac{R_\upsilon(\beta_m,r)}{N(\beta_m)} \times\int_{r=0}^{r_b}\int_{\phi=0}^{2\pi}\int_{r'=0}^{r_{Yb}}\int_{\phi'=0}^{2\pi}R_\upsilon(\beta_m,r')\Phi(\phi-\phi')\psi'_1\psi'_2\psi_1\psi_2 r'rdr'\,d\phi'drd\phi\right) \tag{3d}$$

$$\chi_2(\Omega) = \frac{2k_0\alpha\eta}{\kappa}\left(\frac{\nu_s}{\nu_R}-1\right)\mathrm{Im}\left(\sum_{\upsilon}\sum_{m=1}^{\infty}\frac{4n_0^2\varepsilon_0^2c^2}{\pi(\alpha\beta_m^2-j\Omega)}\frac{R_\upsilon(\beta_m,r)}{N(\beta_m)} \times\int_{r=0}^{r_b}\int_{\phi=0}^{2\pi}\int_{r'=0}^{r_{Yb}}\int_{\phi'=0}^{2\pi}R_\upsilon(\beta_m,r')\Phi(\phi-\phi')\psi'_1\psi'_2\psi_1\psi_2 r'rdr'\,d\phi'drd\phi\right) \tag{3e}$$

In these equations, P_i is optical power, $i = 1, 2$ represent the LP_{01} and LP_{11} modes, respectively. Ω is the offset frequency between the LP_{01} and LP_{11} modes. k_0 is the wave vector of the signal and β_m can be obtained by solving the equation after applying boundary condition as follows: $\beta_m J'_\nu(\beta_m r_b) + J_\nu(\beta_m r_b)h_q/\kappa = 0$.

The coupling coefficients χ_1 and χ_2 denote the thermally-induced refractive index grating originating from the quantum defect (i.e., pump-signal conversion) and the SRS effect (i.e., signal-Raman conversion), respectively. The two gratings can couple power from the fundamental mode to higher order modes, and thus influence the laser beam quality. The quantum-defect induced grating only exists in the active fiber; on the other hand, the SRS-induced grating is present and increases along the entire fiber, starting from the gain fiber in the oscillator and amplifier through the passive fiber used for laser beam delivery.

In commercial multi-kilowatt fiber laser, a 20/400 Yb-doped LMA fiber and the co-pumped scheme are commonly used [20]. Thus, the same configuration was adopted in the simulation model; the laser system used a master oscillator power amplifier (MOPA) layout and the main parameters are listed in Table 1. Besides, we assumed that the Raman content in the laser seed was 0.1% and that the length of the passive fiber, including the tail of cladding power stripper (CPS) and the quartz block head (QBH), was 5 m. Assuming that 2 kW of pump power was injected, the power evolution of the pump light, the signal light, and the Raman light along the entire fiber length are presented in Fig. 1. The power of the Raman light reached 3 W in the end, that is, the Raman content in the output laser was 0.17%. The heat deposition along the fiber was also investigated. The heat generated from the pump-signal conversion and the signal-Raman conversion are plotted in Fig. 2(a) and Fig. 2(b), respectively. It is clear that, the heat deposition due to SRS effects

TABLE 1
Parameters of Test Amplifier

d_{core}	20 μm	λ_s	1064 nm
n_{clad}	1.45	λ_p	976 nm
NA_{core}	0.065	h_q	1000 W/(m^{2}K)
NA_{clad}	0.46	τ	901 μs
N_{Yb}	6.52$\times 10^{25}$ m^{-3}	η	1.2$\times 10^{-5}$ K^{-1}
σ_{ap}	1.77$\times 10^{-24}$ m^2	κ	1.38 W/(Km)
σ_{ep}	1.71$\times 10^{-24}$ m^2	ρ	1.55$\times 10^{6}$ J/(Km^3)
σ_{as}	6.40$\times 10^{-27}$ m^2	P_0	20 W
σ_{es}	3.98$\times 10^{-25}$ m^2	g_R	0.5$\times 10^{-13}$ m/W

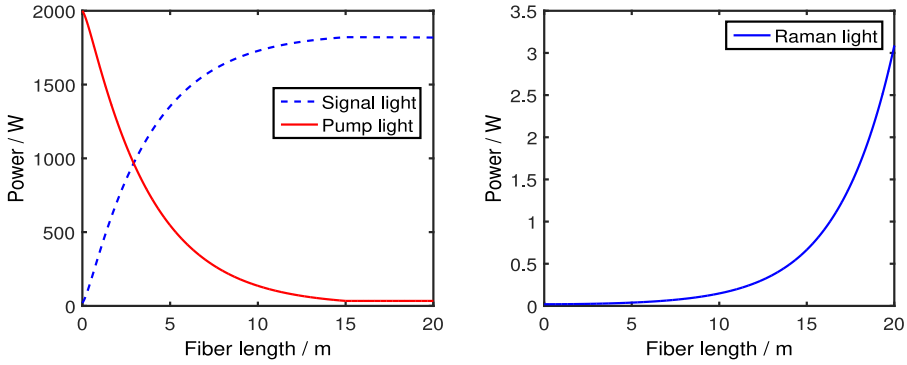

Fig. 1. (a) Power evolution of the signal light and the pump light along the fiber. (b) Power evolution of the Raman light along the fiber.

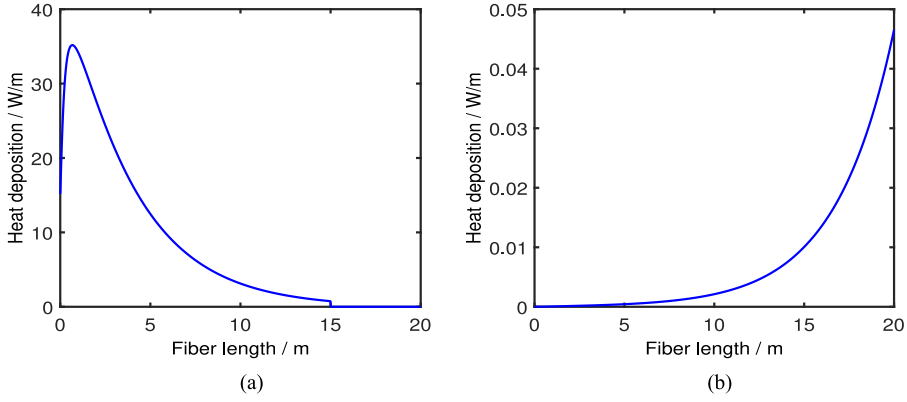

Fig. 2. Evolution of heat deposition due to (a) quantum defect and (b) SRS effect along the fiber.

increased in a nonlinear way along the fiber, composed of 15 m of active fiber and 5 m of passive fiber. In fact, the Raman power and its heat deposition were quite small in this case and, even so, the TMI threshold in our model decreased from 1901 W to 1845 W.

As the length of passive fiber increased, or when the Raman content of the seed was increased, the SRS effect in the laser system became more severe, and the Raman content of the output laser went up, as shown in Fig. 3(b). On the other hand, owing to the increase of the SRS effect, more heat was generated on the fiber, causing the TMI threshold to drop, as shown in Fig. 3(a). Consequently, the TMI threshold decreased dramatically as the Raman content in the seed and the

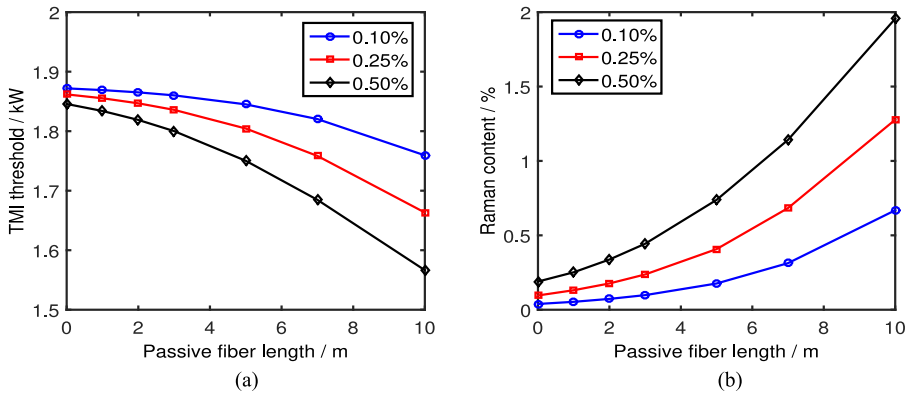

Fig. 3. (a) TMI threshold as a function of passive fiber length for seeds with different injected Raman content. (b) Percentage of Raman content as a function of passive fiber length for seeds with different injected Raman content.

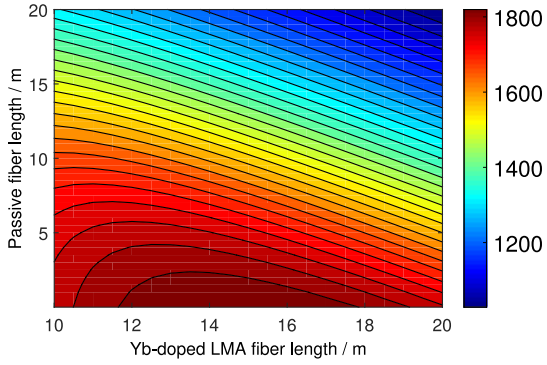

Fig. 4. TMI threshold as a function of active and passive fiber length. The color bar denotes the power of the TMI threshold, expressed in Watts.

passive fiber length were increased. Furthermore, the impact of the length of the active and passive fibers on the TMI threshold was thoroughly investigated, as shown in Fig. 4. It is clear that the TMI threshold decreased as the overall fiber length increased, due to the increase of the Raman effect as well as the increased heat generation. We also found, as shown in Fig. 4, that Yb-doped fibers shorter than a certain value, e.g., 12 m, may result in a low TMI threshold. This might be caused by insufficient pump absorption and the decline of the fiber laser amplification efficiency.

3. Experimental Setup and Results

To investigate the behavior of TMI in co-pumped fiber lasers, a fiber laser system based on the MOPA configuration was developed. The experimental setup is presented in Fig. 5. In the oscillator stage, pump power from a 50 W diode laser (DL) was injected in the cavity via a (2 + 1) $\times$ 1 multi-mode power combiner (MPC); the cavity was built with 4 m of Yb-doped 10/130 double cladding fiber, of which the nominal absorption coefficient was approximately 5 dB/m at 976 nm, and with a proper high reflector (HR) and output coupler (OC) enclosing it to realize a narrow-linewidth multi-longitudinal mode seed laser. After the cavity, a home-made CPS was used to remove unwanted cladding power, and a mode field adapter (MFA) was then employed to minimize insertion losses and to maintain the good beam quality of the seed laser coupled to the power amplifier. In the amplification stage, a co-pumped (6 + 1) $\times$ 1 MPC was used to add up pump power coming from other DLs into a 20/400 Yb-doped fiber (YDF). The active 20/400 fiber had a core numerical aperture of 0.065, which could support transmissions in the LP_{01} and LP_{11} modes. The nominal cladding

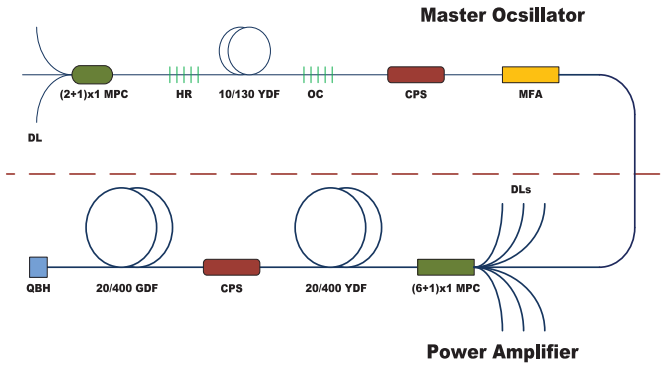

Fig. 5. Experimental setup.

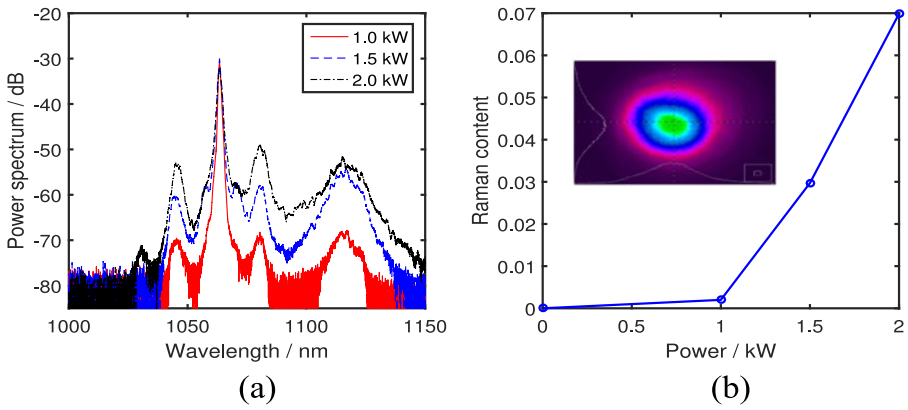

Fig. 6. (a) Spectra of the output laser for 1.0 kW, 1.5 kW, and 2 kW of power, with the passive fiber being 5 m long. (b) Percentage of Raman content as a function of output power, with the inset showing the beam profile of the Raman light.

absorption was approximately 1.2 dB/m at 976 nm, so a 15 m long active fiber was employed to ensure sufficient pump power depletion. Again a home-made CPS, capable of removing 500 W of cladding power, was used afterwards to purify the signal laser in the fiber core, and a QBH was integrated at the end for laser power delivery. The total length of the passive Germanium-doped fiber (GDF), including the parts in the CPS and the QBH, was 10 m.

The output spectra of the laser with the passive fiber length reduced to 5 m are shown in Fig. 6(a). It is clear that as the power of the output laser increased, the Raman content and two other spectral peaks beside the 1064 nm signal (resulting from four-wave mixing) were all enhanced. The percentage of Raman light in the laser output was calculated and is presented in Fig. 6(b), from which the increasing trend of the Raman effect when increasing laser power is also quite obvious. The Raman content in the seed laser was less than 0.1%, but rose to 7% for the final output at 2 kW of power. Compared with the simulation result, which was 0.17%, the growth of the Raman content seems to be more intense in the real case. This may be due to our SRS model neglecting the temporal properties of the seed [21], [22]. In addition, TMI was also analyzed according to the beam profiler measurement results; the threshold value was 1.92 kW, which is in good agreement with the indication of the previous simulation. In fact, it is not apparent whether the Raman or the signal light are affected by TMI, so a long-pass filter with a cut-on wavelength of 1100 nm was inserted before the beam profiler to see pure Raman light. The results, shown in the inset of Fig. 6(b), demonstrate that the Raman light is nearly in single mode; in other words, TMI emerged in the signal light rather than in the Raman light.

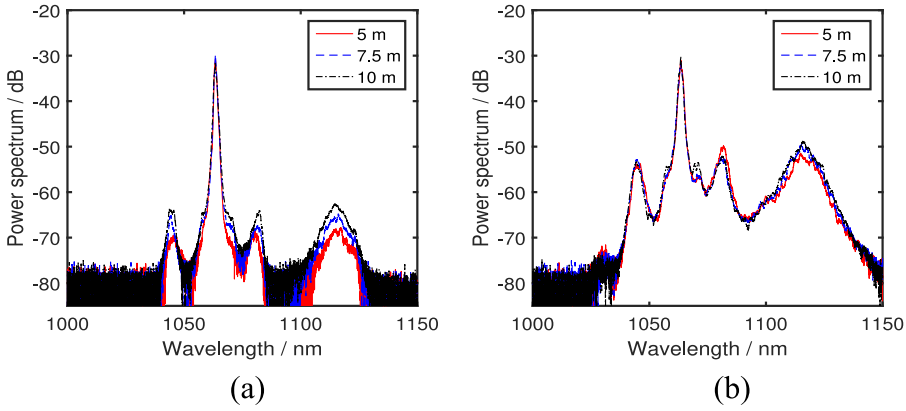

Fig. 7. Spectra of the output laser with passive fibers 5 m, 7.5 m, and 10 m long (a) when the output power was 1 kW and (b) when the power was the TMI threshold.

In order to investigate the impact of the SRS effect on the TMI threshold, the passive fiber between the final CPS and the QBH was cut to reduce its total length from 10 m to 7.5 m, and then to 5 m. The spectra measurements, shown in Fig. 7(a), show a clear decrease in the Raman content. The respective TMI thresholds were 1.72 kW, 1.83 kW, and 1.92 kW, respectively. The output spectra at these powers are plotted in Fig. 7(b), and the Raman content was measured to be 9.1%, 8.8%, and 6.0%, respectively. Our experimental results were in qualitative agreements with the simulation results presented in Fig. 3. Moreover, we observed that the temperature of the passive fiber increased remarkably when the Raman light increased. Similar to the signal-pump quantum defect, heat is generated due to the conversion from signal light to Raman light. Thermally-induced refractive index grating was produced in both active and passive fibers, causing mode coupling from LP_{01} to LP_{11} and a decrease of the TMI threshold. Therefore, it might be effective to suppress the SRS effect (and thus increase the TMI threshold) by shortening the passive fiber length.

4. Discussion

In order to improve the TMI threshold, it is essential to suppress the SRS effect. As indicated in Fig. 4, shortening the length of the active and passive fibers could be effective to mitigate the SRS effect, but this might limit the application of fibers for lasers requiring delivery at long distances. It should be mentioned that, unlike the laser system presented in the paper, the TMI threshold is independent of the fiber length in Raman fiber lasers [11]. According to previous research [12], the counter-pumped scheme applied to fiber lasers could also suppress SRS and thus increase the TMI threshold. This is because the valid fiber lengths in which signal-to-Raman conversion could take place are normally shorter and the gain saturation is effectively enhanced when using the counter-pumped architecture.

Moreover, using fibers with a larger mode field diameter could be an effective way to mitigate SRS, which can be derived from theoretical simulations results presented in Fig. 8. For core diameters greater than 25 μm, lengthening the passive fiber had less of an impact on the TMI threshold, and the Raman content increments could almost be neglected. However, fibers of larger core diameters could guide more modes, which would result in a substantial decrease of the TMI threshold. In addition, a spectral model was developed to predict the impact of the seed laser on the SRS effect, indicating that SRS could be suppressed by increasing the bandwidth of the fiber Bragg gratings or by reducing the seed power [22]. However, increasing the bandwidth of the seed would limit the power scaling of narrow-linewidth lasers. On the other hand, decreasing of the seed power might reduce the TMI threshold because it would worsen the gain saturation [12]. Therefore, there is usually a trade off when suppressing the SRS effect and the TMI effect simultaneously.

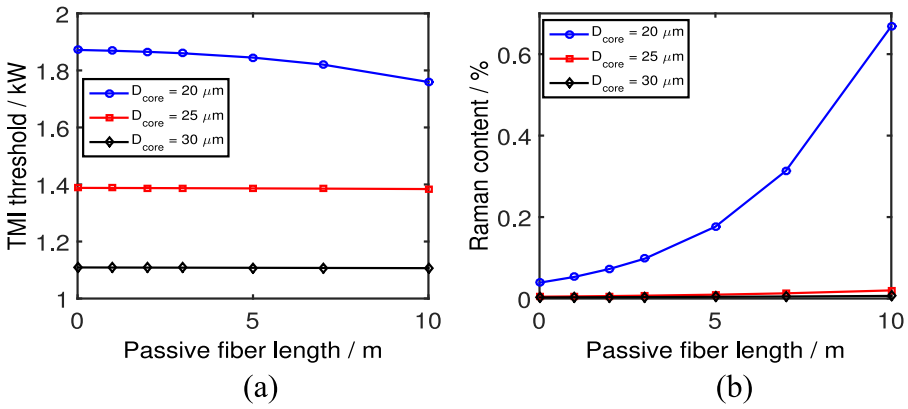

Fig. 8. (a) TMI threshold as a function of passive fiber length for different core diameters. (b) Raman content as a function of passive fiber length for different core diameters.

5. Conclusion

In this work, the impact of the SRS effect on the TMI threshold was investigated both theoretically and experimentally. The quantum defect between the signal light and the Raman light results in a thermally-induced refractive index grating, which may induce the TMI effect. Simulation results verified that the TMI threshold could be significantly reduced as the Raman content in the laser output increases. A similar trend was also found in our experimental results. Besides, we proved that TMI emerges in the signal light rather than in the Raman light. Moreover, methods to mitigate the SRS effect were also discussed, indicating that laser systems require a careful design to properly balance the SRS and TMI effects.

The lateral resolution of the image obtained by numerical reconstruction was assessed utilizing a wavelet image decomposition and image correlation. The best lateral resolution obtained with a high NA recording, 164 nm, represents an improvement of more than a factor two relative to previously published results.

Acknowledgment

The authors wish to thank the anonymous reviewers for their valuable suggestions.

References

[1] T. Eidam *et al.*, "Femtosecond fiber CPA system emitting 830 w average output power," *Opt. Lett*, vol. 35, no. 2, pp. 94–96, 2010. [Online]. Available:

[2] T. Eidam *et al.*, "Experimental observations of the threshold-like onset of mode instabilities in high power fiber amplifiers," *Opt Exp.*, vol. 19, no. 14, pp. 13218–13224, 2011. [Online]. Available: http://www.ncbi.nlm.nih.gov/pubmed/21747477

[3] C. Jauregui, T. Eidam, J. Limpert, and A. Tunnermann, "The impact of modal interference on the beam quality of high-power fiber amplifiers," *Opt. Exp.*, vol. 19, no. 4, pp. 3258–3271, 2011. [Online]. Available: http://www.ncbi.nlm.nih.gov/pubmed/21369148

[4] A. V. Smith and J. J. Smith, "Mode instability in high power fiber amplifiers," *Opt. Exp.*, vol. 19, no. 11, pp. 10180–10192, 2011. [Online]. Available: http://www.opticsexpress.org/abstract.cfm?URI=oe-19–11-10180

[5] K. Brar *et al.*, "Threshold power and fiber degradation induced modal instabilities in high-power fiber amplifiers based on large mode area fibers," *Proc. SPIE*, vol. 8961, 2014, Art. no. 89611R. [Online]. Available: http://dx.doi.org/10.1117/12.2042261

[6] H.-J. Otto, N. Modsching, C. Jauregui, J. Limpert, and A. Tünnermann, "Impact of photodarkening on the mode instability threshold," *Opt. Exp.*, vol. 23, no. 12, 2015, Art. no. 15265.

[7] C. Jauregui, H.-J. Otto, S. Breitkopf, J. Limpert, and A. Tünnermann, "Optimizing high-power yb-doped fiber amplifier systems in the presence of transverse mode instabilities," *Opt. Exp.*, vol. 24, no. 8, pp. 7879–7892, 2016. [Online]. Available: http://www.opticsexpress.org/abstract.cfm?URI=oe-24–8-7879

[8] B. Ward, "Theory and modeling of photodarkening-induced quasi static degradation in fiber amplifiers," *Opt. Exp.*, vol. 24, no. 4, pp. 3488–3501, 2016. [Online]. Available: http://www.opticsexpress.org/abstract.cfm?URI=oe-24–4-3488
[9] J. Lgsgaard, "Static thermo-optic instability in double-pass fiber amplifiers," *Opt. Exp.*, vol. 24, no. 12, pp. 13429–13443, 2016. [Online]. Available: http://www.opticsexpress.org/abstract.cfm?URI=oe-24–12-13429
[10] Y. Changgeng, L. Petit, J. J. Koponen, I. N. Hu, and A. Galvanauskas, "Short-term and long-term stability in ytterbium-doped high-power fiber lasers and amplifiers," *IEEE J. Sel. Top. Quantum Electron.*, vol. 20, no. 5, Sep./Oct. 2014, Art. no. 0 903 512. [Online]. Available: ¡Go to ISI¿://INSPEC:14249089
[11] S. Naderi, I. Dajani, J. Grosek, and T. Madden, "Theoretical and numerical treatment of modal instability in high-power core and cladding-pumped raman fiber amplifiers," *Opt. Exp.*, vol. 24, no. 15, pp. 16550–16565, 2016. [Online]. Available: http://www.opticsexpress.org/abstract.cfm?URI=oe-24–15-16550
[12] Z. Li *et al.*, "Experimental demonstration of transverse mode instability enhancement by a counter-pumped scheme in a 2 kw all-fiberized laser," *Photon. Res.*, vol. 5, no. 2, pp. 77–81, 2017. [Online]. Available: http://www.osapublishing.org/prj/abstract.cfm?URI=prj-5–2-77
[13] A. V. Smith and J. J. Smith, "Increasing mode instability thresholds of fiber amplifiers by gain saturation," *Opt. Exp.*, vol. 21, no. 13, pp. 15168–15182, Jul. 2013. [Online]. Available: http://www.opticsexpress.org/abstract.cfm?URI=oe-21–13-15168
[14] Y. Wang, "Stimulated raman scattering in high-power double-clad fiber lasers and power amplifiers," *Opt. Eng.*, vol. 44, no. 11, pp. 114202–114202–12, 2005. [Online]. Available: http://dx.doi.org/10.1117/1.2128147
[15] H. Zhang, H. Xiao, P. Zhou, X. Wang, and X. Xu, "High power yb-raman combined nonlinear fiber amplifier," *Opt. Exp.*, vol. 22, no. 9, pp. 10248–10255, May 2014. [Online]. Available: http://www.opticsexpress.org/abstract.cfm?URI=oe-22–9-10248
[16] Q. Xiao *et al.*, "Bidirectional pumped high power raman fiber laser," *Opt. Exp.*, vol. 24, no. 6, pp. 6758–6768, Mar. 2016. [Online]. Available: http://www.opticsexpress.org/abstract.cfm?URI=oe-24–6-6758
[17] K. R. Hansen, T. T. Alkeskjold, J. Broeng, and J. Laegsgaard, "Theoretical analysis of mode instability in high-power fiber amplifiers," *Opt. Exp.*, vol. 21, no. 2, pp. 1944–1971, 2013. [Online]. Available: http://www.ncbi.nlm.nih.gov/pubmed/23389177
[18] I.-N. Hu, C. Zhu, C. Zhang, A. Thomas, and A. Galvanauskas, "Analytical time-dependent theory of thermally induced modal instabilities in high power fiber amplifiers," *Proc. SPIE*, vol. 8601, 2013, Art. no. 860 109.
[19] T. Rumao, M. Pengfei, W. Xiaolin, Z. Pu, and L. Zejin, "Mitigating of modal instabilities in linearly-polarized fiber amplifiers by shifting pump wavelength," *J. Opt.*, vol. 17, no. 4, 2015, Art. no. 045504. [Online]. Available: http://stacks.iop.org/2040–8986/17/i=4/a=045504
[20] Z. Huang *et al.*, "Spectral broadening in high-power yb-doped fiber lasers employing narrow-linewidth multilongitudinal-mode oscillators," *Appl. Opt.*, vol. 55, no. 2, pp. 297–302, Jan. 2016. [Online]. Available: http://ao.osa.org/abstract.cfm?URI=ao-55–2-297
[21] T. Schreiber, A. Liem, R. Eberhardt, J. Limpert, and A. Tnnermann, "Analysis of stimulated raman scattering in CW kw fiber oscillators," *Proc. SPIE*, vol. 8961, 2014, Art. no. 89611T. [Online]. Available: http://dx.doi.org/10.1117/12.2039869
[22] W. Liu, P. Ma, H. Lv, J. Xu, P. Zhou, and Z. Jiang, "General analysis of SRS-limited high-power fiber lasers and design strategy," *Opt. Exp.*, vol. 24, no. 23, pp. 26715–26721, 2016. [Online]. Available: http://www.opticsexpress.org/abstract.cfm?URI=oe-24–23-26715